REDISTRIBUTION OF GLOBAL PRECIPITATION OBSERVED IN THE EL NIÑO EVENTS BY USING MULTI-TEMPORAL REMOTE SENSING

L. Vasiliev

Institute of Geography, Russian Academy of Sciences, Staromonetny 29, Moscow 119017, Russia - vasiliev@igras.geonet.ru

Commission VII, WG

KEYWORDS: El Niño, precipitation, mass flow rate, wavelet transform, singularity

ABSTRACT:

According to model predictions, the most significant manifestation of climate change would be an acceleration of the global water cycle, leading to increased global precipitation. Knowledge of global precipitation is needed in order to investigate the existence of significant global trends in the rate of the water cycle. Quantitative measurement of the time and space distribution of precipitation is the next highest climate research priority after atmospheric temperature and moisture. Satellite remote sensing is the only means to acquire global rainfall data. The multi-satellite one degree daily global precipitation data spanning the years 1996-2004 has been used to meet challenges associated with regularity and perturbations in global precipitation. Wavelet is a tool used to study regularity. The most notable features are periodicity in an amount of precipitation and the total rainy area. They are independent variables. We introduce the global daily precipitation mass flow rate. The striking manifestations of El Niño are clear examples of the linkage between large-scale anomaly and changes in global weather process. Analysis of the time series of global precipitation that twice underwent perturbations during the El Niño events revealed new properties of the mass flow rate behaviour. To what extent are variations in precipitation related to global change remains to be learned.

1. INTRODUCTION

According to model predictions, the most significant manifestation of climate change would be an acceleration of the global water cycle, leading to increased global precipitation. Knowledge of global precipitation is needed in order to investigate the existence of significant global trends in the rate of the water cycle. Quantitative measurement of the time and space distribution of precipitation is the next highest climate research priority after atmospheric temperature and moisture. Satellite remote sensing is the only means to acquire global rainfall data. The striking manifestations of El Niño are clear examples of the linkage between large-scale anomaly and changes in global weather process. To what extent are variations in precipitation related to global change remains to be learned.

Global precipitation produces complex behaviour, which is both highly organised and chaotic. Complexity means that we have structure with variations. These structures vary widely in size and duration. What is seen often depends on the size of the observer (Goldefeld & Kadanoff, 1999). In a chaotic precipitation it is hard to predict which variation will arise in a given place and time. But precipitation contains regularities as well. To extract physical knowledge from such a complex system one must focus on the right level of description to catch the phenomena. The inclusion of too many parameters will obscure the desired quantitative understanding. Apparently there are no general laws for complexity. Each complex system is different so for exploration we use experimental technique based on multi-temporal remote sensing. Intermittency seems to be a feature of precipitation only on a local scale in the presence of the boundary conditions. In recent years, considerable study has been devoted to applicability of Self-organised criticality (SOC) to rainfall (Bak et al., 1987). SOC in precipitation and avalanche like dynamics make sense only in a restricted space and may yield a successful description of the small-scale structure. But this description is irrelevant for the global scale paper length because the global precipitation forms in space-time an infinite cluster (Vasiliev, 2002).

The El Niño Southern Oscillation is the main driver of the change in precipitation patterns all around the world. By studying the global precipitation patterns over the last 7 years has been established that El Niño drastically modifies rainfall space-time structure in many regions (Curtis & Adler, 2000). The multi-satellite one degree daily precipitation spanning the years 1996-2004 has been used to meet challenges associated with regularity and perturbations in global precipitation. In theoretical practical studies on the environmental processes the notation of regularity has been increasing in importance. However, we do not even know exactly how individual El Niño events come into existence. The paper explains the effect of punctuated equilibrium observed in the El Niño events during 1996 – 2004. The initial data are images with spatial resolution 1°x 1° in latitude and longitude that have one day temporal resolution of precipitation (Huffman et al., 2001).

2. LOCATION AND STABILITY OF ANOMALIES

The seven-year time series of global precipitation, with two El Niño events (1997 – 1998) and (2002 – 2003) gives an idea about the stability of its space time effects on the precipitation redistribution on the planetary level. The stability of the mechanism of the dynamic space-time structure of global precipitation during an El Niño event was estimated by way of comparison of rain redistribution of 1997 – 1998 and 2002 – 2003 and shown in Figure 1. Note that the latest event was much weaker than the previous. The comparison of two space-time structures is an evidence for a relative stability of the

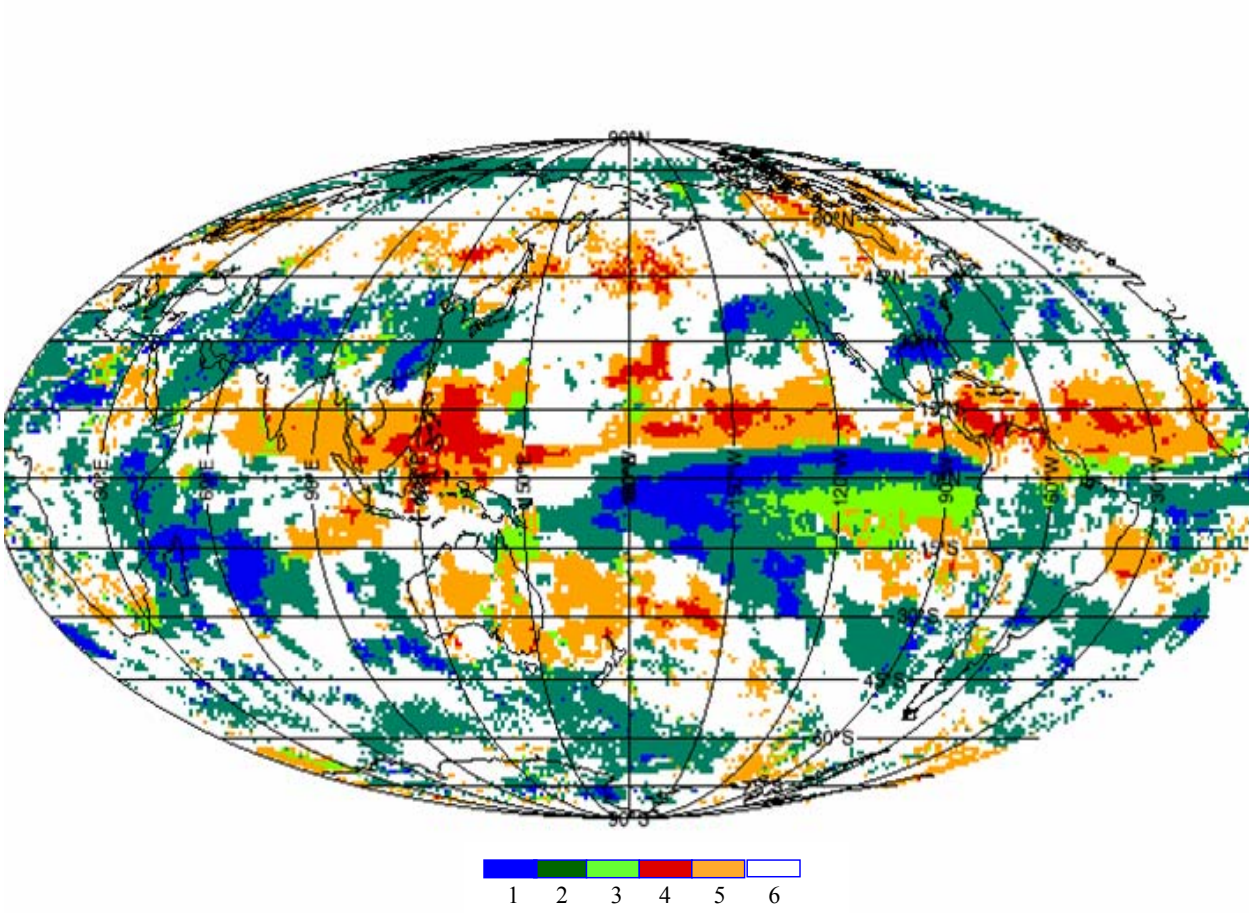

Figure 1. Composite of anomalies in global precipitation during the El Niño events in 1997 – 1998 and 2002 – 2003. Colour combinations made with two images show: The positive (1) and negative (4) anomalies which have occurred in two events. Areas (2) and (5) designate a location where positive or negative anomalies have occurred only once during one of the two events. The anomaly at the area (6) did not appear. An unanticipated result (3) was the sign change of an anomaly observed in a strip alongside the Equator near the west cost of South America. Results of pair wise comparison across the two El Niño effects are tabulated in the table 1.

global precipitation response to the external driving force. Table 1 summarises some of the results.

Type of anomalous redistribution	Relative area
No El Niño effect P_0	0.49
Stable positive anomaly P_+	0.05
Unstable positive anomaly $P_{0/+}, P_{+/0}$	0.26
Stable negative anomaly P_-	0.03
Unstable negative anomaly $P_{0/-}, P_{-/0}$	0.14
Anomaly sign reversal $P_{+/-}$	0.03

Table 1. Comparison of areas and locations of precipitation anomalies during the two El Niño events

To a certain extent about a half of the planet surface may be affected by the El Niño events. The P_+ and P_- values characterize the area of nuclei of positive and negative anomalies. Being a function of El Niño intensity, about 0.4 more of the Earth's surface may find itself within the areas of positive or negative anomalies. Quite unexpected is behaviour of precipitation within the positive anomaly area during the weak El Niño event, which results in the anomaly sign reversal. Changes in the precipitation behaviour during this El Niño event occurred over 35% of the Earth's surface: with positive anomalies generated over 27% and negative, over 10% of the surface. The rate of growth of positive and negative anomalies A are described by the power law dependence on time t

$$\frac{dA}{dt} \propto t^{-1.07} \text{ and } \frac{dA}{dt} \propto t^{-1.0} \qquad (1)$$

Rapid decrease of anomaly growth is obvious. It should also be added that simultaneously within anomalies the direction of the zonal transport of specific humidity is drastically changing: in positive anomalies the direction of trade winds changes through 120°, in negative, through 180°.

The natural global precipitation oscillation is recognizable in its interannual variability in the total amount of local precipitation. The variation refers to the sum of year-to-year local precipitation without El Niño affecting. In the normal course of events, the positive and negative precipitation anomalies form small random clusters. Their annual distribution in space is not stable, but the total area constantly covers 8 percent of the Earth

surface on equal terms. There is a corresponding significant increase in size of the unstable anomalies during El Niño $P_{0/+}$, $P_{+/0}$ = 0.26 – 0.04, $P_{0/-}$,$P_{-/0}$=0.14 – 0.04.

El Niño's impact around the world affected 40 percent of the Earth, provided more positive anomalies and increase of global precipitation at 18 percent. The non-significant anomalies location are not evenly distributed in space but are characterised instead by patterns related to large ocean warm currents, Amazon and the South Ocean, which are characterised as relatively homogeneous. However, these regions of the world are differently affected by the El Niño event: the positive precipitation anomalies are most strongly related to the ocean current over the North Atlantic and Amazon, but there is a decrease in precipitation in the North Pacific.

3. PUNCTUATED EQUILIBRIUM IN PRECIPITATION

Global precipitation could be regarded as an example of self organised criticality in the environment, meaning that the system is in the state of punctuated equilibrium. In case El Niño is present and the sea surface temperature exceeds a certain threshold (> 2°C) a perturbation develops in precipitation over wide scale range. Local disturbances bring about positive and negative anomalies. Changes on the planetary level occur due to large-scale water mass shift.

Space time series of global precipitation explains to a grate extent the effect of punctuated equilibrium in the complex atmospheric system. We now use two time series of measurements at the global scale: daily precipitation volume *P(t)* and the area *A(t)* that precipitation occupies during a day in discrete time interval t. These non correlated variables are independent and form a 2D-Gaussian (*P, A*). Each of them, if taken alone, does not show any signs of regularity. We introduce a precipitation mass flow rate, *M=AP/t*, which determines the amount of precipitation, *P* passing through an area *A* in unit time *t* (here within 24 hours). It is reasonable to use *M*-function since it permits one to operate simultaneously two independent variables *P, A,* and to characterise the global daily precipitation rate. To analyze the behaviour of this function in order to detect signs of regularity, we employ wavelet transform (Foufoula-Georgiou & Kumar 1994, Kaiser 1994).

Most of the basic wavelet theory has been worked up. However, more effort is still required to permit its use for practical analysis of experimental time series. The key role here belongs to the selection of the wavelet basis function. To determine the true signatures of regularity and to interpret them a wavelet should be adapted to a given time series for an accurate pattern recognition. For comparison, Figures 2 and 3 show the same wavelet analysis of the precipitation flow rate time series *M(t)*. The wavelet power spectrum of *M(t)* by using a derivative of Gaussian (DOG), *m* = 6, is shown in Figure 2. A picture produced by using the Morlet wavelet is shown in Figure 3.

The most noticeable difference is the fine scale structure using the DOG. This is because the derivative of Gaussian is real valued and captures both the positive and negative oscillations of the time series as separate peaks in wavelet power. The Morlet wavelet is both complex and contains more oscillations than the DOG, and hence the wavelet power combines both positive and negative peaks into a single broad peak. Overall, the same features appear in both plots, approximately at the

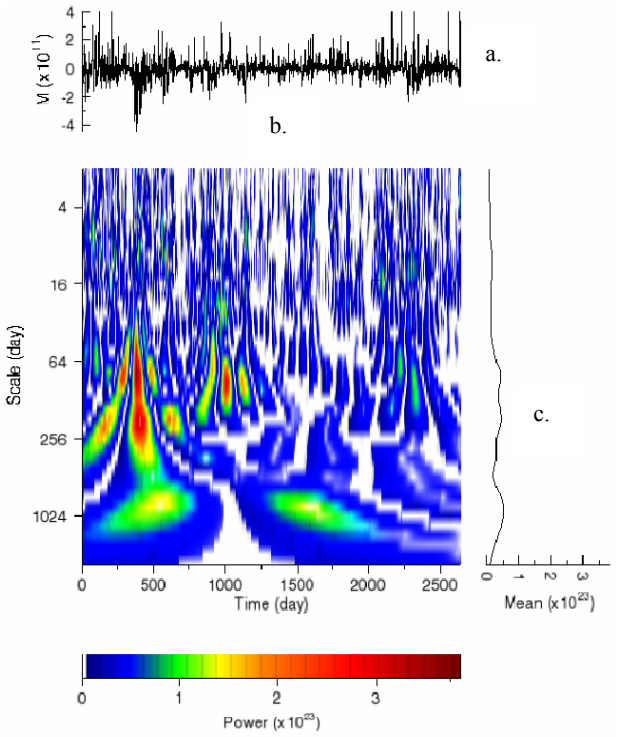

Figure 2. (a) Global precipitation mass flow rate used for the wavelet analysis. (b) The local wavelet power spectrum of (a) using the derivative of a Gaussian. (c) The time-averaged wavelet spectrum.

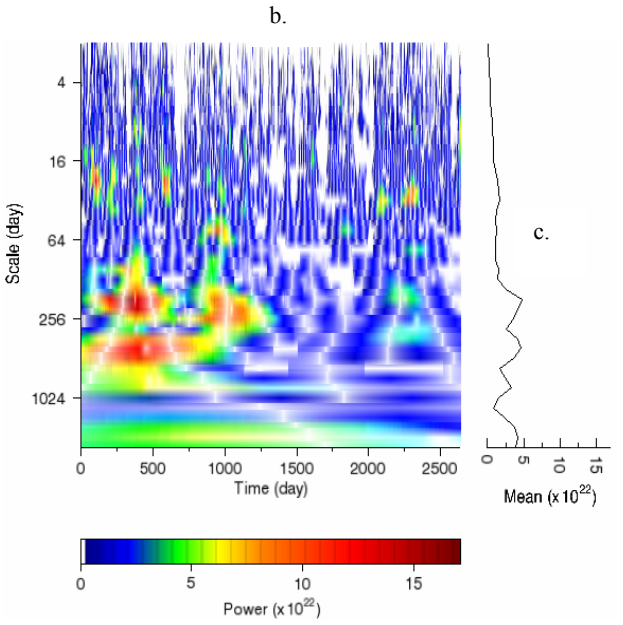

Figure 3. (b) The local wavelet power spectrum of the same as (a) in Figure 2 using the wavelet Morlet. Light lines show the location of a zero phase. (c) The time-averaged wavelet spectrum.

same locations, and with the same power. Comparing Figures 2 and 3, DOG is narrower in time-space, yet broader in spectral-space than the Morlet. Thus, in Figure 2 the peaks appear very sharp in the time direction, yet are more elongated in the scale direction. Finally, the relationship between time-averaged wavelet spectrum of DOG and Morlet is very different for the

two functions. An examination of wavelet transforms shows that the choice of wavelet function was not critical, and one function gave the same qualitative results as another. The qualitative estimate and the *M(t)* time series interpretation coincide in both cases and permit the following conclusion. In the 1996 – 2003 years the El Niño impact on the global precipitation varied and lasted from 19 to 6–7 months. During this period the wavelet power spectrum has significantly higher power at the wavelet scale about 250 days. Within the interval [1300, 2000 days] in the absence of any outer source of excitation the two wavelet transforms show no marked signs of regularity in the precipitation mass flow rate.

The wavelet power spectrum (WPS) of the precipitation mass flow rate with a derivative of a Gaussian obviously localizes along the time axis the position of maxima and minima of the relative power in the precipitation at a certain scale and a certain time. However, the character of changes in WPS seriously depends on the El Niño power. The impact of the event during 1997 – 1998 continued about 1000 days. The *M(t)* time series permits identification of two periods of that interval. The frequency localisation of the Morlet wavelet power spectrum is precisely determined. The duration of the periods is about 250 and 500 days, respectively. For 1000 days the interaction of a stationary process and perturbing process induces perturbation of precipitation of mass flow rate at 250 and 500 day periods. Zero phases in 250 and 500 day periods are shifted around 200 days. Similar effect also repeats during a weaker El Niño manifestation in 2002 – 2003 but this time the magnitude of the WPS is much lower.

4. CENTRE OF GRAVITY MOVEMENT

The large scale longitudinal shift of precipitation is recorded as their centre of gravity (COG) trajectory (Vasiliev 2004). In the El Niño periods the COG of global precipitation shifts eastward in the equatorial plane around 40°–50°, displacing the precipitation pattern in the Pacific Ocean. Signatures of punctuated equilibrium in the precipitation distribution are determined from the wavelet transform for the time series of the centre of gravity of precipitation *L(t)* and shown in Figure 4. Large scale displacements of precipitation bringing about punctuated equilibrium are determined from two wavelet transforms for *L(t)* time series. Equilibrium is recovered in about 1000 days with two 500 day periods thus the duration of the intense of El Niño impact on a large scale water mass displacement is twice the duration of the anomalous rise of the sea surface temperature. The 2002 – 2003 El Niño impact was similar to that but the WPS of the trajectory of the COG is much lower, which follows from both wavelet transforms with DOG and the Morlet wavelet. Equilibrium distortion manifested itself at least in precipitation mass flow rate perturbation on the planetary level and in the formation of anomalies. However, the events had different duration. Wavelet transforms of gravity showed that the responses of two variables to external driving force impact agree sufficiently well in time and in frequency domain. One precipitation flow rate and longitudinal displacement of the centre should not try to interpret the values of the local wavelet power spectrum in Figure 4 with a scale / period longer than 1000 day for the 2645 day time series.

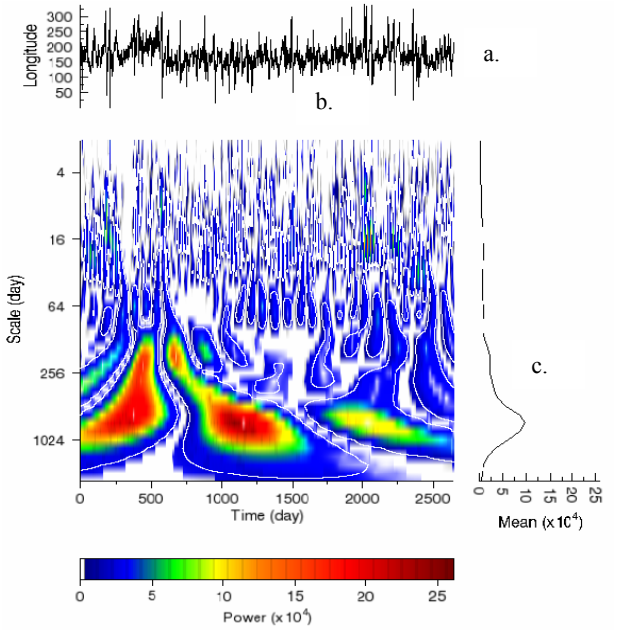

Figure 4. The local wavelet power spectrum of the COG longitudinal location. (a) Time series of longitudinal coordinates of COG. (b) The local wavelet power spectrum of (a) by using a derivative of a Gaussian (*m*=6). Regions limited by white outlines correspond to 99% confidence level for local WPS. (c) The time-averaged wavelet spectrum.

5. SINGULARITY STRUCTURE OF GLOBAL PRECIPITATION

Global precipitation is a process with non-periodic behavior and local variations. During an external force, such as the El Niño event, there are discontinuity and rapid changes in the time series which are called singularities. Regularity in global precipitation is a quite complex concept and we will try to explain in using the continuous wavelet transform (CWT). It is sufficient for our purpose to state that the CWT can be used for characterizing the Hölder singularities in the time series of global precipitation. Using the CWT is crucial in obtaining the Hölder exponent (HE). The CWT contains the original signal's frequency spectrum for each instant time. The Hölder exponent can then be extracted from each frequency spectrum and provides a measure of signal regularity *H(t)* as a function of time (Gonçalvès and Flandrin, 1992).

Let us take the wavelet transform $W^{(n)} f$ of the function f in $t=t_0$ with the wavelet of at least n vanishing moments, i.e. orthogonal to polynomials up to degree n:

$$\int_{-\infty}^{+\infty} t^m \psi(t) dt = 0 \quad \forall t,\ 0 \le t < n \tag{2}$$

For the sake of illustration, let us assume the function f can be characterised by Hölder exponent $H(t_0)$ in t_0, and f can be locally described as

$$f(t)_{t_0} = c_0 + c_1(t-t_0) + \ldots + c_n(t-t_0)^n + C\left|t-t_0\right|^{H(t_0)}$$

Its wavelet transform $W^{(n)}f$ with the wavelet at least n vanishing moments now becomes

$$W^{(n)}f(a,t_0)=\frac{1}{a}\int C|t-t_0|^{H(t_0)}\psi\left(\frac{t-t_0}{a}\right)dt=C|a|^{H(t_0)}\psi(t')dt'$$

Therefore, we have the following power law proportionality for the wavelet transform of the (Hölder) singularity of $f(t_0)$

$$W^{(n)}f(a,t_0)\sim|a|^{H(t_0)} \qquad (3)$$

Therefore the Hölder exponent of a singularity can be evaluated as a scaling exponent of the wavelet transform coefficient $Wf(a,t_0)$ for $a\to 0$.

Figure 5 shows the local Hölder exponent for the time series of precipitation mass flow rate *M(t)*. It can be seen that precipitation mass flow rate is characterised by trends and discontinuities that give a particular shape to the process. The measure of singularity provided by the Hölder exponent can be used to detect discontinuities in precipitation mass flow rate. The more continuous the process, the closer the value is one and a Hölder exponent of 0 indicates the presence of singularity (discontinuity). The process discontinuity can be located in time. Thus around a given point, the faster wavelet decreases when the scale *a* goes to 0, the more regular *f* is around the point. As seen in Figure 5 the singularities in the time series of precipitation mass flow rate *M(t)* are not isolated but densely packed during the El Niño events. The Hölder exponent time series detected the discontinuities in global precipitation were not obvious in the time signal or the frequency spectrum.

This result leads us to the general conclusion of the redistribution of global precipitation. A discontinuity in the mass flow rate from the El Niño impact introduces energy content at high frequency spectrum, causing the HE to approach zero or a negative value. The mean value for the HE associated with the undamaged mass flow rate is $<H(t)>=0.20$-0.24. In comparison with this the HEs, affected by the El Niño three different types of values in the frequency distribution can be distinguished: i) The greatest energy at relatively low frequencies during El Niño. ii) El Niño attenuation introducing energy content at high frequencies into the frequency spectrum, causing singularity and the HE approach zero or a negative value $<H(t)\leq 0$. The duration of this process is about 8 months. iii) A slowdown in disturbance of global precipitation and its regularisation. The HE raises sharply to 1. There is a remarkable similar behaviour of the Hölder exponent during both El Niño events over the range of time scales in 1997-1998 and 2002-2003.

The comparison between the Hölder exponent time series of precipitation mass flow rate and the longitudinal trajectory of the centre of gravity supports the conclusion that the El Niño impact on global precipitation. Figure 6 shows that discontinuities in HE time series of mass flow rate and trajectory of the centre of gravity and location of singularity are similar only during the strong El Niño spanning the years October 1996 - June 1999. After that the regularity of the

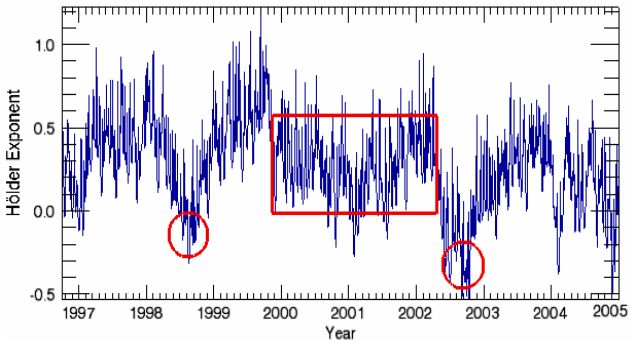

Figure 5. Time series with local Hölder exponent evaluated from global precipitation mass flow rate from the figure 2a(1). The El Niño impact in 1997-1998 and 2002-2003 indicates the presence of strong singularity circled in red. The HEs without impacts are shown in the rectangle.

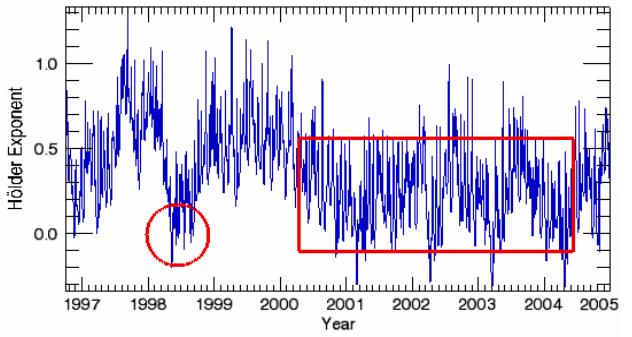

Figure 6. Time series with local Hölder exponent evaluated from the trajectory of the centre of gravity of global precipitation from the figure 3(1). The El Niño impact in 1997-1998 and 2002-2003 indicates the presence of strong singularity circled in red. The HEs without impacts are shown in the rectangle.

trajectory is about $<H(t)\leq 0.20$. Note: one should bear in mind that singularity in a global precipitation process is not a singularity of random noise.

6. CONCLUSIONS

El Niño is one of the main sources of external driving force impact on global precipitation. This phenomenon changes its space time structure and gives birth to irregular climatic rhythms. Analysis of the 1996 – 2004 global precipitation that twice underwent perturbations during the El Niño events revealed new properties of the precipitation mass flow rate and the trajectory of their centre of gravity. A remarkable property of the CWT is its ability to characterise the local regularity of global precipitation. The Hölder exponent greatly simplified the interpretation of a change in global precipitation behaviour. The measure of non-stationarity provided by the Hölder exponent has been used to detect singularity in precipitation during El Niño. They are not obvious in the signal or the frequency spectrum. The duration of perturbation due to El Niño was significantly longer than an increased SST lasted. The singularities and regularisation in precipitation during the El Niño impact redistributed the space-time structure with a period up to 18 months around 40% of the Earth surface affected by El

Niño. The precipitation anomalies expanded around the world but they are unevenly distributed. Areas of stable positive and negative anomalies cover up to 10% of the surface. The positive anomalies are more than twice as much. The research offers new insight into how global precipitation might be influenced by the Earth radiation imbalance. Progress in understanding of the complex environmental system has been achieved by using the more aggregated variables on the large scale level: precipitation mass flow rate and dynamics of their centre of gravity. Variables on such level could be derived only relying upon regular multi-temporal remote sensing. The efficiency of a similar space technology urges the world community to launch the Global Precipitation Measurement mission in the future which would study year-to-year changes in the hydrological cycle.

ACKNOLEDGEMENTS

The 1DD data were provided by the NASA/Goddard Space Flight Center's Laboratory for Atmospheres, which develops and computes the 1DD as a contribution to the GEWEX Global Precipitation Climatology Project.

REFERENCES

Bak, P., Tang, C. & Wiesenfeld, K. 1987. Self-organized criticality: an explanation of 1/f noise. *Phys. Rev. Lett.* Vol. 59: 381-384.

Curtis, S. and Adler, R. 2000. ENSO indexes based on patterns of satellite-derived precipitation. *J. Climate.* Vol. 13: 2786-2793.

Foufoula-Georgiou, E. and Kumar, P. (eds.). 1994. Wavelets in Geophisics. Academic Press, San Diego, CA, 373 pp.

Goldenfeld, N. and Kadanoff, L. 1999. Simple lessons from complexity. *Science, 284,* 87-89.

Gonçalvès, P. and Flandrin P. 1992. Scaling exponents estimation from time-scale energy distributions. In IEEE Int. Conf. on Acoust., Speech and Signal Proc. ICASSP-92, V. 157-V. 160

Huffman, G.J., Adler, R.F. et al. 2001. Global Precipitation at one-degree daily resolution from multi-satellite observations. *Journal of Hydrometeorology. 2, 36-50.*

Kaiser, G. 1994. A Friendly Guide to Wavelets. Birkhäuser, Cambridge, MA, 300 pp.

Vasiliev, L. 2002. Spatio-temporal pattern formation in rainfall from remote sensing observations. In G. Begni (ed.). *Observing our environment from space*. Balkema, Rotterdam, 159-165.

Vasiliev, L. 2004. Redistribution of global precipitation observed in the El Niño events by using remote sensing. In R. Goossens (ed.). *Remote Sensing in Transition*. Millpress, Rotterdam, 313-318.

Vasiliev, L., Kachalin, A., Tyuflin, A. 2005. Interrupted equilibrium in global precipitation during El Niño periods. Doklady Earth Sciences, Vol. 403A, No. 6, 966-971